crystals

MDPI

Article

(2*E*)-2-[1-(1,3-Benzodioxol-5-yl)-3-(1*H*-imidazol-1-yl) propylidene]-*N*-(2-chlorophenyl)hydrazine carboxamide: Synthesis, X-ray Structure, Hirshfeld Surface Analysis, DFT Calculations, Molecular Docking and Antifungal Profile

Reem I. Al-Wabli [1,*], Alwah R. Al-Ghamdi [1], Suchindra Amma Vijayakumar Aswathy [2], Hazem A. Ghabbour [3], Mohamed H. Al-Agamy [4,5], Issac Hubert Joe [2] and Mohamed I. Attia [1,6,*]

1 Department of Pharmaceutical Chemistry, College of Pharmacy, King Saud University, P.O. Box 2457, Riyadh 11451, Saudi Arabia; toto24se@hotmail.com
2 Center for Molecular Biophysics Research, Mar Ivanios College, Nalanchira, Thiruvanthapuram 695015, India; aswathyrs86@gmail.com (S.A.V.A.); hubertjoe@gmail.com (I.H.J.)
3 Department of Medicinal Chemistry, Faculty of Pharmacy, Mansoura University, Mansoura 35516, Egypt; ghabbourh@yahoo.com
4 Department of Pharmaceutics, College of Pharmacy, King Saud University, P.O. Box 2457, Riyadh 11451, Saudi Arabia; malagamy@KSU.EDU.SA
5 Microbiology and Immunology Department, Faculty of Pharmacy, Al-Azhar University, Cairo 11884, Egypt
6 Medicinal and Pharmaceutical Chemistry Department, Pharmaceutical and Drug Industries Research Division, National Research Centre (ID: 60014618), El Bohooth Street, Dokki, Giza 12622, Egypt
* Correspondence: ralwabli@KSU.EDU.SA (R.I.A.-W.); mattia@ksu.edu.sa (M.I.A.); Tel.: +966-11-805-2620 (R.I.A.-W.); +966-146-77337 (M.I.A.)

Received: 3 January 2019; Accepted: 29 January 2019; Published: 4 February 2019



Abstract: Life-threatening fungal infections accounts for a major global health burden especially for individuals suffering from cancer, acquired immune deficiency syndrome (AIDS), or autoimmune diseases. (2*E*)-2-[1-(1,3-Benzodioxol-5-yl)-3-(1*H*-imidazol-1-yl)propylidene]-*N*-(2-chlorophenyl) hydrazinecarboxamide has been synthesized and characterized using various spectroscopic tools to be evaluated as a new antifungal agent. The (*E*)-configuration of the imine moiety of the title molecule has been unequivocally identified with the aid of single crystal X-ray analysis. The molecular structure of compound **4** was crystallized in the monoclinic, $P2_1/c$, a = 8.7780 (6) Å, b = 20.5417 (15) Å, c = 11.0793 (9) Å, β = 100.774 (2)°, V = 1962.5 (3) Å^3, and Z = 4. Density functional theory computations have thoroughly explored the electronic characteristics of the title molecule. Moreover, molecular docking studies and Hirshfeld surface analysis were also executed on the title compound **4**. The in vitro antifungal potential of the target compound was examined against four different fungal strains.

Keywords: Crystal structure; Imidazole; Benzodioxole; Semicarbazone; DFT

1. Introduction

The dramatic increase in the morbidity due to life-threatening fungal infections accounts for a major health burden worldwide, particularly for those individuals suffering from cancer, AIDS, or autoimmune diseases [1–3]. The presence of few drug targets in the eukaryotic fungal cells that are not shared with human cells limits the availability of selective antifungal agents, as compared with

the anti-bacterials [4]. The emergence of resistance to the available antifungal agents as well as their serious side effects led to the necessity for the search for new alternative antifungal therapies [5].

Imidazole and/or triazole moieties constitute the core pharmacophore part of most azoles, which are used as a first-line treatment for various fungal infections [6]. Azoles inhibit competitively the sterol biosynthesis via inhibition of fungal lanosterol 14α-demethylase (CYP51) leading to a hindering of the normal fungal growth [7]. The presence of two carbons linking the azole pharmacophore part and an aromatic residue is a common feature in the available antifungal azoles. Whereas, the reported antifungal candidates bearing a propyl bridige between the aromatic moiety and the azole fragment are limited [8–10].

Semicarbazones are formally derived from the condensation of certain semicarbazide with the appropriate aldehydes or ketones. While semicarbazones have received less attention than their respective thiosemicarbazones, they became versatile ligands and drawn the attention of a number of researchers in the scientific community during the last fifteen years. Semicarbazones have the ability to coordinate with various metal ions and form complexes due to the existence of oxygen and nitrogen donor atoms in their core structure. In addition, they mostly occur in the keto form in the solid state, while they exhibit a keto-enol tautomerism in the solution state [11]. Semicarbazones displayed significant antibacterial, anticonvulsant, antioxidant, and antifungal activities and their structures can be further elaborated to prepare various bioactive heterocyclic compounds [12,13]. Moreover, metal complexes of semicarbazones exhibited a broad spectrum bioactivities like the activities toward smallpox, protozoa, influenza, trypanosomiasis, certain kinds of tumors, malaria, and fungi [14].

In addition, literature search exposed that benzodioxole fragment occurs in a large number of biologically active molecules including antimicrobials [15–17].

In a continuation of our efforts to obtain new potent antifungal compounds [18–22], we were inspired to design and synthesize (2*E*)-2-[1-(1,3-benzodioxol-5-yl)-3-(1*H*-imidazol-1-yl) propylidene]-*N*-(2-chlorophenyl)hydrazinecarboxamide to be examined as a new antifungal agent. The title compound comprises three pharmacophore parts, namely imidazole, semicarbazone, and benzodioxole with a three-carbon bridge separating benzodioxole and imidazole fragments with the aim to get new potent drug-like antifungal hybrid. Single crystal X-ray analysis and different spectroscopic techniques assured the assigned chemical structure of the title compound as well as the (*E*)-configuration of its imine functionality. In addition, the electronic characters and molecular geometry of the title molecule were explored with the aid of density functional theory (DFT) computations. Molecular docking simulations and Hirshfeld surface analysis were also executed for the title compound **4**. The in vitro antifungal profile of the target compound was examined against four different fungal strains.

2. Experimental

2.1. General

Gallenkamp melting point apparatus was harnessed to measure melting point of compound **4** and it is uncorrected. Nuclear magnetic resonance (NMR) measurements were executed in DMSO-d_6 with the aid of Bruker NMR spectrometer at 500 MHz for ^{1}H and 125.76 MHz for ^{13}C at the Research Center, College of Pharmacy, King Saud University, Saudi Arabia. δ-values (ppm) were used to represent chemical shifts in relation to tetramethylsilane (TMS) as an internal standard. Mass spectrum of compound **4** was recorded using Agilent Quadrupole 6120 LC/MS (Agilent Technologies, Palo Alto, CA, USA) implemented with ESI (Electrospray ionization) source. Silica gel precoated aluminum thin layer chromatography plates with fluorescent indicator at 254 nm were secured from Merck (Darmstadt, Germany) and illumination with UV light source (254 nm) accomplished visualization.

2.2. Synthesis

Synthesis of (2*E*)-2-[1-(1,3-benzodioxol-5-yl)-3-(1*H*-imidazol-1-yl)propylidene]-*N*-(2-chloro phenyl)hydrazinecarboxamide (**4**)

Few drops of glacial acetic acid were added to a stirred reaction mixture containing ketone **3** (0.24 g, 10 mmol) and *N*-(2-chlorophenyl)hydrazinecarboxamide (1.86 g, 10 mmol) [23], in absolute ethyl alcohol (15 mL) and stirring was continued atambient temperature for 18 h. Ethyl alcohol was removed under vacuum and the residue was purified by re-crystallization from ethyl alcohol to afford the corresponding semicarbazones **4** as colorless crystals suitable for X-ray analysis. Yield 0.51 g (51%); white powder m.p. 163–165 °C; IR (KBr): ν (cm^{-1}) 3676 (NH), 3018, 2902, 1753 (C=O), 1508 (C=N), 1442, 1352, 754; ^{1}H-NMR (DMSO-d_6): δ (ppm) 3.29 (t, *J* = 7.0 Hz, 2H, –CH_2–CH_2–N), 4.11 (t, *J* = 7.0 Hz, 2H, –CH_2–CH_2–N), 6.08 (s, 2H, -O-CH_2-O-), 6.86 (s, 1H, –N–CH=C*H*–N=), 6.94 (d, *J* = 8.0 Hz, 1H, Ar–H), 7.10 (t, *J* = 7.5 Hz, 1H, Ar–H), 7.25 (d, *J* = 8.5 Hz, 1H, Ar–H), 7.27 (s, 1H, –N–C*H*=CH–N=), 7.36 (t, *J* = 7.5 Hz, 1H, Ar-H), 7.41 (s, 1H, Ar-H), 7.51 (d, *J* = 7.5 Hz, 1H, Ar-H), 7.63 (s, 1H, –N–C*H*=N–), 8.25 (d,*J* = 7.5 Hz, 1H, Ar-H), 9.12 (s, 1H, NH), 10.57 (s, 1H, NH); ^{13}C-NMR (DMSO-d_6): *δ*(ppm) 28.9 (C-2′), 42.8 (C-3′), 101.9 (–O–CH_2–O–),106.3, 108.5, (Ar–CH), 119.9 (C-5″), 121.1, 121.2, 122.9, 124.3, 128.4, 128.7, 129.6, 131.3, 135.7 (Ar-CH, Ar–C, C-4″), 137.8 (C-2″), 145.9, 148.3, 148.7, 153.4 (Ar–C, C=O, C=N); MS *m*/*z* (ESI): 412.1 $[M + H]^+$, 413.0 $[(M + 1) + H]^+$, and 414.1 $[(M + 2) + H]^+$.

2.3. Crystal Structure Determination

Single crystals of the title compound **4** were achieved via slow evaporation of the ethyl alcohol solution of the pure compound at ambient temperature. Bruker APEX-II D8 Venture area diffractometer (Bruker, Billerica, MA, USA) implemented with graphite monochromatic Mo *K*αradiation, λ = 0.71073 Å at 293 (2) K, was employed for data collection. Bruker SAINT was harnessed for data reduction and cell refinement and SHELXT [24] was utilized for structure solving. Full-matrix least-square technique was utilized for final refinement with the aid of anisotropic thermal data for non-hydrogen atoms on *F*. CCDC 1,875,003 contains the supplementary crystallographic data for compound **4** can be obtained free of charge from the Cambridge Crystallographic Data Centre via www.ccdc.cam.ac.uk/data_request/cif.

2.4. Quantum Chemical Calculations

Quantum mechanical methods helped by the functional B3LYP/6-311+G were used to obtain the vibrational wavenumbers of the semicarbazone **4** and to optimizeits structure [25]. The theoretical investigations of the semicarbazone **4** were carried out with the aid of Gaussian 09W software [26]. The exchange and correlation functions embedded in the software with the occurrence of the density functional theory (DFT) are vital to get results closer to the experimental data. The distribution of assignments of the simulated wavenumbers were evaluated with the aid of vibrational energy distribution analysis (VEDA) 4 program [27].Crystal Explorer 3.1 was utilized to generate fingerprint plots and Hirshfeld surface map of the semicarbazone **4** [28]. NBO 3.1 program supported natural hybrid calculations, natural populations, and natural bonding orbital investigations [29].

2.5. Antifungal Activity

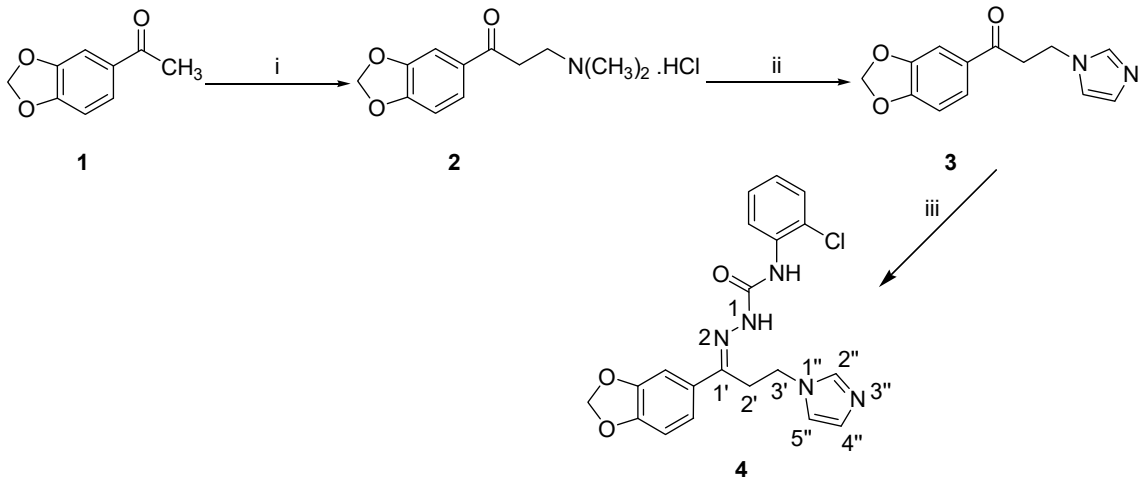
The MICs of the semicarbazone **4** towards various fungal strains were inspected according to literature method [20].

3. Results and Discussion

3.1. Chemistry

The synthetic procedure to prepare the target compound **4** is decorated in Scheme 1. The ketone **3** [19] was successfully obtained according to the previously reported method

using acetophenone derivative **1** as a starting material. Subsequently, the semicarbazide *N*-(2-chlorophenyl)hydrazinecarboxamide [23] was allowed to react with compound **3** to yield the target semicarbazones **4** in an acceptable yield.



Scheme 1. Synthesis of the target semicarbazone **4**. *Reagents and conditions*: **(i)** $HN(CH_3)_2 \cdot HCl$, $(CH_2O)_n$, conc. HCl, ethanol, reflux, 2 h; **(ii)** Imidazole, water, reflux, 5 h; **(iii)** *N*-(2-Chlorophenyl)hydrazinecarboxamide, ethanol, acetic acid, rt, 18 h.

3.2. Crystal Structure of the Semicarbazone **4**

In compound **4**, $C_{20}H_{18}ClN_5O_3$, the crystallographic information and refinement data are presented in Table 1. Table 2 illustrates the chosen bond angles and bond lengths. Figure 1 displayed the asymmetric unit which contains one independent molecule. All the bond angles and bond lengths occur in normal ranges [30]. The molecules are packed together in the crystal structure by one classical hydrogen bond and three non-classical hydrogen bonds, as presented in Figure 2 and Table 3. The 1,3-benzodioxole plane makes dihedral angles of 16.91° and 52.91° with a chlorophenyl ring and imidazole ring, respectively.

Table 1. X-ray experimental details of the semicarbazone **4**.

Crystal Data	
Molecular formula	$C_{20}H_{18}ClN_5O_3$
Mr	411.84
Crystal system, space group	Monoclinic, $P2_1/c$
Temperature (K)	293
a, *b*, *c* (Å)	8.7780 (6), 20.5417 (15), 11.0793 (9)
β (°)	100.774 (2)
V (Å^3)	1962.5 (3)
Z	4
Radiation type	Mo *Kα*
μ (mm^{-1})	0.23
Crystal size (mm^3)	0.33 × 0.19 × 0.11
Data Collection	
Diffractometer	Brucker APEX-II D8 venture diffractometer
Absorption correction	Multi-scanSADABS Bruker 2014
T_{min}, T_{max}	0.954, 0.962
No. of measured, independent and observed [I> 2σ(I)] reflections	28076, 4511, 2424
R_{int}	0.095
Refinement	
$R[F^2 > 2\sigma(F^2)]$, $wR(F^2)$, *S*	0.060, 0.137, 1.04
No. of reflections	4511
No. of parameters	270
No. of restraints	0
H-atom treatment	H atoms treated by a mixture of independent and constrained refinement
$\Delta\rho_{max}$, $\Delta\rho_{min}$ (e Å^{-3})	0.18, −0.29

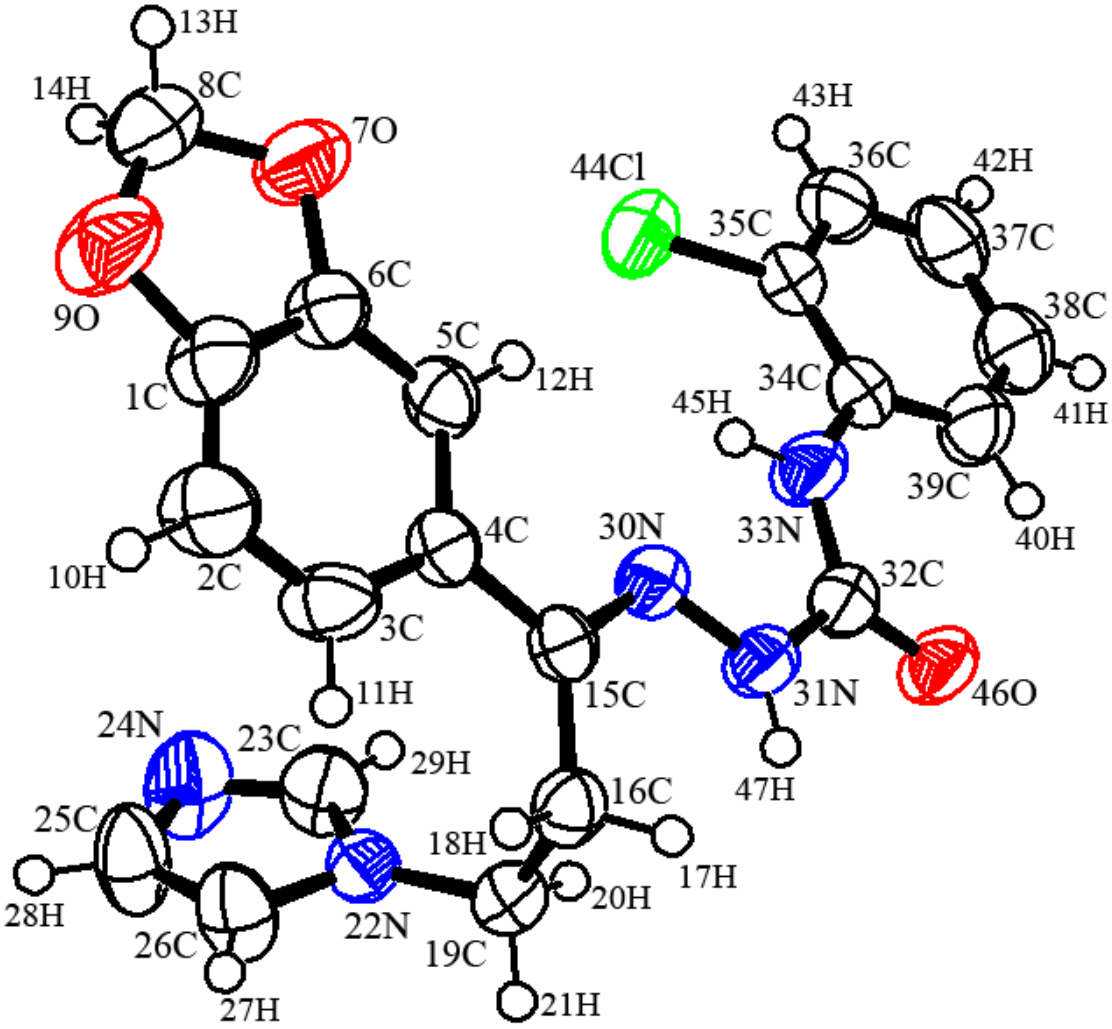


Figure 1. Oak ridge thermal ellipsoid plot diagram of the semicarbazones **4** drawn at 50% ellipsoids for non-hydrogen atoms.

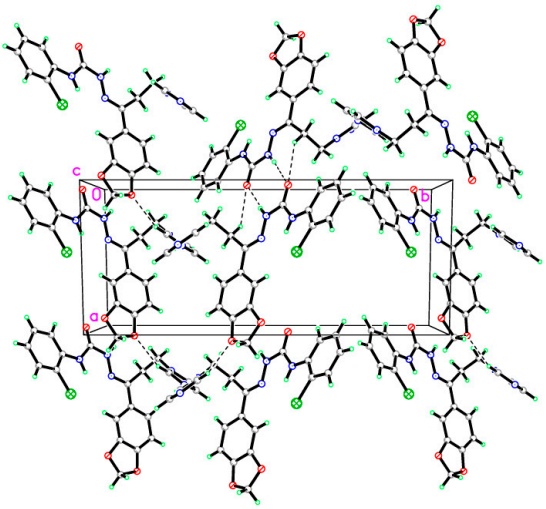


Figure 2. Molecular packing of the semicarbazone **4** manifesting hydrogen bonds which are drawn as dashed lines.

Table 2. Geometric parameters (Å, °) of the semicarbazone **4**.

Atom	Bond Length/Angle	Atom	Bond Length/Angle
Cl44–C35	1.736 (3)	N22–C26	1.359 (3)
O7–C6	1.377 (3)	N24–C23	1.300 (4)
O7–C8	1.416 (3)	N24–C25	1.350 (4)
O9–C1	1.372 (3)	N30–N31	1.378 (3)
O9–C8	1.422 (4)	N30–C15	1.288 (3)
O46–C32	1.224 (3)	N31–C32	1.360 (3)
N22–C19	1.454 (3)	N33–C32	1.361 (3)
N22–C23	1.351 (3)	N33–C34	1.403 (3)
C6–O7–C8	105.8 (2)	N30–C15–C4	116.0 (2)
C1–O9–C8	105.4 (2)	N30–C15–C16	123.5 (2)
C19–N22–C23	126.9 (2)	N22–C19–C16	114.3 (2)
C19–N22–C26	127.8 (2)	N22–C23–N24	112.9 (3)
C23–N22–C26	105.3 (2)	N24–C25–C26	111.2 (3)
C23–N24–C25	104.3 (3)	N22–C26–C25	106.4 (2)
N31–N30–C15	119.1 (2)	N31–C32–N33	114.8 (2)
N30–N31–C32	119.4 (2)	O46–C32–N31	120.6 (2)
C32–N33–C34	127.9 (2)	O46–C32–N33	124.6 (3)
O7–C6–C1	109.2 (2)	N33–C34–C39	124.1 (3)
O7–C6–C5	128.4 (2)	N33–C34–C35	118.4 (2)
O9–C1–C2	128.8 (3)	Cl44–C35–C34	119.5 (2)
O9–C1–C6	109.9 (2)	Cl44–C35–C36	118.8 (2)
O7–C8–O9	107.5 (2)		

Table 3. Hydrogen-bond geometry (Å) of the semicarbazone **4**.

D–H···A	D–H	H···A	D···A	D–H···A
N31–H4N31···O46i	0.85(3)	2.06(3)	2.896(3)	169(3)
C16–H17B···O46i	0.9700	2.5100	3.207(3)	129.00
C23–H29A···O9ii	0.9300	2.4500	3.301(4)	152.00
C26–H27A···N24iii	0.9300	2.4900	3.326(4)	150.00
C39–H40A···O46	0.9300	2.3000	2.886(4)	121.00

Symmetry codes: (i) −x−2, −y−1, −z−1; (ii) x−1, y, z; (iii) x, −y−3/2, z−1/2.

3.3. Structural Geometry Analysis

The geometry of the semicarbazone **4** was optimized with the aid of DFT theory at B3LYP/6-311++G (d,p) level of basis set by Gaussian 09 program package. The atom numbering scheme is displayed in Figure 3. No constraints on the bond lengths, bond angles or dihedral angles were observed in the calculations and all atoms were free to optimize. Table 4 illustrates the relevant optimized geometrical parameters for the semicarbazone **4** along with its experimental values. There is a difference in values from crystallographic data which might be arise from the fact that theoretical results belong to gaseous phase (isolated molecule), whereas the experimental results belong to solid phase. A statistical correlation graph showing the gaseous and solid phase bond lengths is depicted in Figure S1 with R^2 value of 0.97233.

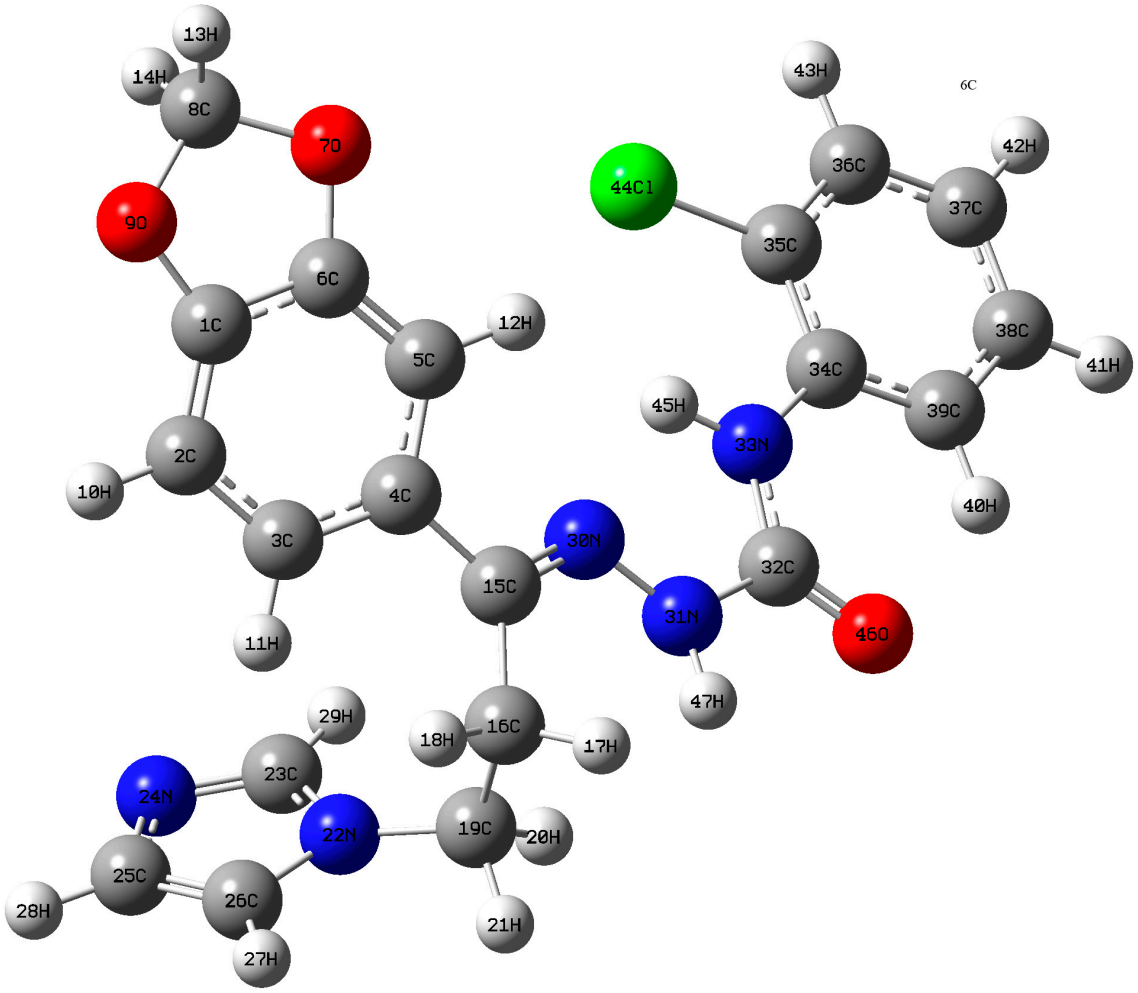


Figure 3. Atom numbering scheme of optimized semicarbazone **4** structure.

The title molecule bears a chlorophenyl moiety connected with a benzodioxole ring through a hydrazinecarboxamide bridge. Connection was extended to theimidazole ring through an ethylene group. Computational geometry optimization of the title molecule revealed that the global energy minimum for the non-planar structure was obtained by 1732.9189 Hartree. The calculated bond lengths of C3–H11, C2–H10, C5–H12 of the benzodioxole ring are 1.0816, 1.0822, and 1.0811 Å, respectively. The shortening of C5–H12 might beowing to the presence of intramolecular C5–H12 ··· N30 hydrogen bonding and it is significantly shorter than the van der Waals radii (2.4104 Å).

The angle of 95.83° between C5–H12 ··· N30 is also within the angle limit manifesting C–H ··· N intramolecular hydrogen bonding. The C–N bond lengths C32–N31 (1.4042 Å) and C32–N33 (1.3875 Å) are shorter than the normal C–N bond length of 1.480 Å. This discrepancy could be attributed to the conjugation of Pi-type electrons of the carbonyl group and nitrogen atom, allowing the electrons to smear out along the C–N bond. Table 4 displayed bond lengths of C3–C4 and C4–C5 in the benzodioxole ring as well as C34–C35, C34–C39 in the chlorophenyl ring which are significantly longer than the other C–C bond lengths in both rings. This is due to the intramolecular charge transfer (ICT) between two rings through hydrazinecarboxamide moiety. DFT calculations indicates a decrease in the endocyclic angles C3–C4–C5 and C35–C34–C39 by 0.76° and 2.42°, respectively, from the normal endocyclic angle of 120° supporting intramolecular charge transfer interactions.

Table 4. Selected optimized parameters for the semicarbazone **4**.

Parameters	DFT	Exp.	Parameters	DFT	Exp.
Bond lengths\Å			**Dihedral Angles\°**		
C1–C2	1.3751	1.356	C5–C4–C15–N30	–0.51	–1.54
C1–C6	1.3954	1.371	C3–C4–C15–N30	179.97	178.01
C2–C3	1.4053	1.392	C15–N30–N31–C32	174.78	176.1
C2–H10	1.0822	0.931	N30–N31–C32–N33	–174.29	–2.89
C3–C4	1.4011	1.378	N32–C32–N33–C34	–178.49	176.6
C3–H11	1.0816	0.931	C32–N33–C34–C39	–1.04	–1.54
C4–C5	1.4189	1.378	C32–N33–C34–C35	179.15	165.48
C4–C15	1.4852	1.480	C4–C15–C16–C19	–88.51	101.58
C5–C6	1.3701	1.359	C15–C16–C19–N22	–175.16	–76.52
C5–H12	1.0811	0.930	C16–C19–N22–C26	–73.22	–78.94
C15=N30	1.2889	1.2881	C16–C19–N22–C23	103.09	101.11
N30–N31	1.3524	1.3781	Bond Angles\°		
C32–N31	1.4042	1.378	C5–C4–C15	121.79	121.74
C32–N33	1.3875	1.402	C3–C4–C15	118.89	119.62
C34–N33	1.4016	1.362	C3–C4–C5	119.33	122.40
C34–C35	1.4072	1.396	N33–C34–C35	118.58	118.36
C34–C39	1.4035	1.389	N33–C34–C39	123.84	124.08
C35–C36	1.3873	1.378	C35–C34–C39	117.58	117.56
C36–C37	1.3918	1.368			
C37–C38	1.3925	1.370			
C38–C39	1.3908	1.380			
C39–C34	1.4035	1.389			

3.4. Natural Bond Orbital Analysis

The NBO calculations were performed using the NBO 3.1 program [29] as implemented in the Gaussian 09 package at the DFT level. It is proved that NBO analysis is an efficient approach for the chemical interpretation of hyperconjugative interactions within the molecule. Additionally, it can be used to explain the electron density transfer (EDT) from the filled lone electron pairs of n(Y) of the "Lewis base" Y into the unfilled antibond σ*(X–H) of the "Lewis acid" X–H in X–H ··· Y hydrogen bonding systems. In addition, NBO analysis can be exploited to elucidate inter and intramolecular hydrogen bonding as well as intermolecular charge transfer in organic molecules.

The intramolecular C–H ··· N hydrogen bonding was formed due to the overlap between n1(O) and σ*C–H which results in intramolecular charge transfer (ICT) causing stabilization of the system. These interactions lead to an increased electron density of the C–H antibonding orbital, which strengthens the C–H bond. In addition, NBO analyses confirmed C5–H12 ··· N30 intramolecular hydrogen bonding formed by the overlap between a lone pair n1(N30) and σ*C5–H12 antibonding orbitals with stabilization energy of 4.40 kcal/mol. Other important interactions are displayed in Table 5.

3.5. Natural Population Analysis

Atomic charges and electron distribution within a molecule can be effectively calculated with the aid of natural population analysis (NPA) [31]. Figure 4 clearly illustrates the atomic charges of the semicarbazone **4** obtained by NPA. The hydrogen atoms of the semicarbazone **4** exhibited net positive charges. The atoms H45 and H47 manifested more positive charge than the other hydrogen atoms owing to their connection to nitrogen atoms. Among the hydrogen atoms of the chlorophenyl and benzodioxole ring, H12 showed the highest positive charge, being involved in C–H···N intramolecular hydrogen bonding. Moreover, the all carbon atoms manifested negative charges except C1, C6, C8, C15, C23, C32, and C34 owing to their connection to nitrogen or oxygen atoms. These findings suggest that the N and O atoms are the preferred sites for protonation. C32 isthe most positively charged atom, while N33 is the most negatively charged one. On the other hand, C35 possesses the lowest negative

charge, as compared with the other carbon atom in the phenyl moiety owing to its connection to the chlorine atom.

Table 5. Second-order perturbation theory analysis of Fock matrix in NBO basis for the semicarbazone **4**.

Donor (*i*)		Acceptor (*j*)		*E*(2) [a] kcal/mol	*E*(*j*)-*E*(*i*) [b] (a.u.)	*F*(*i*,*j*) [c] (a.u.)
NBO	Occupancy	NBO	Occupancy			
σ(C1–C2)	1.97467	σ*(C1–C6)	0.03968	4.48	1.27	0.068
σ(C1–C2)	1.97467	σ*(C1–O9)	0.02853	3.66	0.34	0.032
σ(C1–C2)	1.97467	σ*(C1–O7)	0.03253	1.47	1.07	0.035
σ (C1–C6)	1.97447	σ*(C1–C2)	0.02065	4.65	1.35	0.071
σ (C1–C6)	1.97447	σ*(C15–N30)	0.01622	1.51	0.76	0.032
σ (C1-O9)	1.98708	σ*(C35–Cl44)	0.03389	0.53	3.49	0.039
σ(C2–H10)	1.97906	σ*(C37–H42)	0.01319	0.58	0.79	0.019
σ(C3–C4)	1.97383	σ*(C1–O9)	0.02853	12.75	0.31	0.056
σ(C3–C4)	1.97383	σ*(C2–C3)	0.02065	6.45	0.17	0.078
σ(C3–C4)	1.97383	σ*(N24–C25)	0.01083	38.23	0.18	0.074
π(C3–C4)	1.69506	π*(C1–C2)	0.02065	0.56	3.68	0.041
π(C3–C4)	1.69506	π*(C25–H28)	0.01691	33.36	4.07	0.356
π(C5–C6)	1.70385	π*(C1–C2)	0.02065	14.57	0.47	0.075
π(C5–C6)	1.70385	π*(C34–C35)	0.46482	0.66	0.45	0.016
n1(N30)	1.90915	σ*(C5–H12)	0.01401	4.40	0.82	0.055
n1(N33)	1.70147	σ*(N31–C32)	0.08922	13.15	0.46	0.069

[a]: *E*(2) means energy of stabilization interactions; [b]: Energy difference between donor-to-acceptor, *i* and *j* NBO orbitals; [c]: *F*(*i*,*j*) is the Fock matrix element between *i* and *j* NBO orbitals.

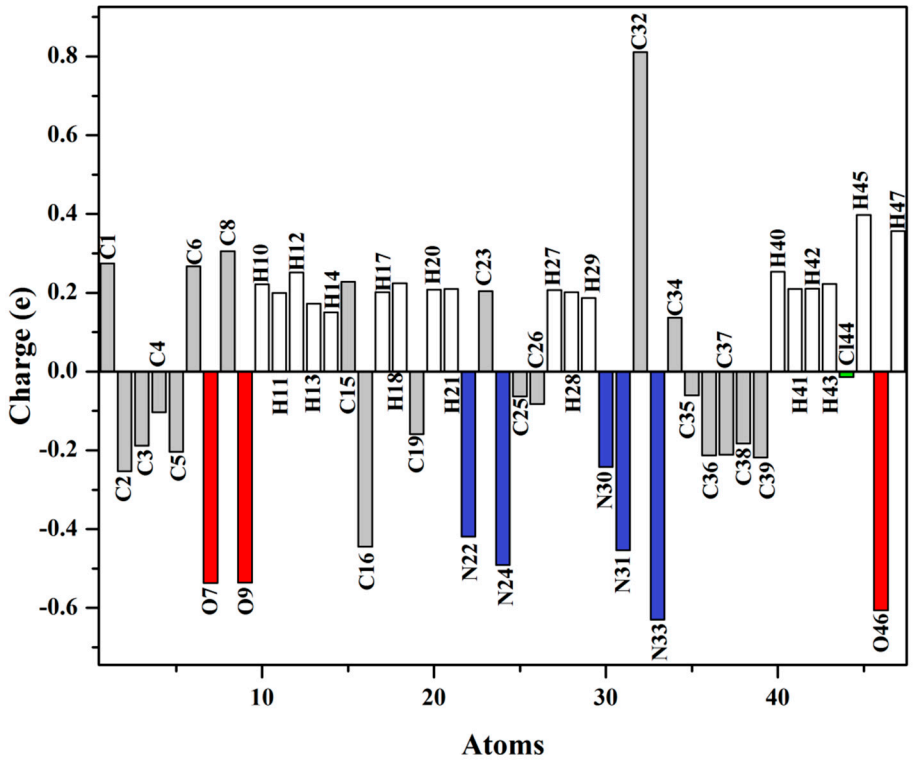


Figure 4. Charge distribution on the atoms of the semicarbazone **4**.

3.6. Frontier Molecular Orbital Analysis

The kinetic stability and chemical reactivity of a molecule could be examined through the energy gap between its HOMO (highest occupied molecular orbital) and its LUMO (lowest unoccupied molecular orbital) [32]. The B3LYP/6-311++G(d,p) level of theory was utilized to calculate the energy gap for the semicarbazone **4** and Figure 5 illustrates the graphical representation of its frontier molecular orbitals. The electron distribution is scattered in HOMO over the benzodioxole ring, the

hydrazinecarboxamide moiety, and is slightly upon the chlorophenyl ring, whereas the LUMO is mainly disseminated over the benzodioxole fragment. The electron density is transferred in the HOMO→LUMO transition from the chlorophenyl fragment to the benzodioxole moiety through the hydrazine carboxamide bridge. This transition illustrates the charge transfer from the electron-donor functionalities to electron-acceptor fragments via a π-conjugated path. The FMO (frontier molecular orbital) energy gap of the semicarbazone **4** was found to be 4.23 eV (HOMO energy = −6.007 eV, LUMO energy = −1.777 eV). This energy gap leads to charge transfer within the semicarbazone **4**, which could promote its bioactivity.

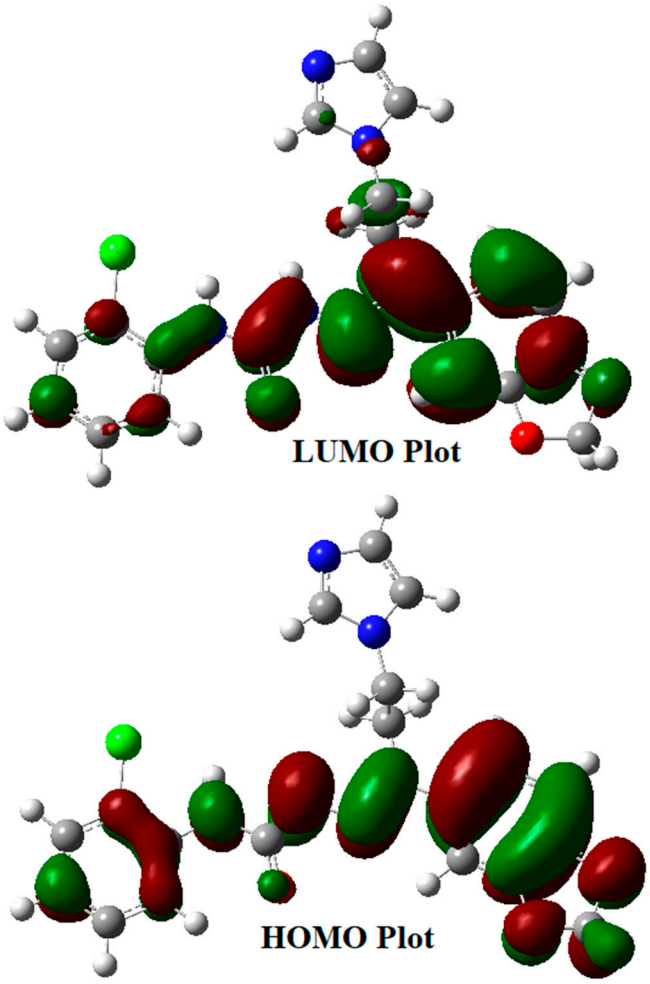


Figure 5. Frontier molecular orbitals of the semicarbazone **4**.

3.7. Molecular Docking Simulations

Gaussian 09 program was used to optimize the structure of the semicarbazones **4** with the aid of the density functional theory using [26]. AutoDock Tools-1.5.4 implemented in MGL Tools-1.5.4 package was harnessed to carry out molecular docking investigations [33]. The fungal RNA Kinase (PDB ID: 5U32) target protein was chosento perform the current docking analysis [34]. The three-dimensional (3D) coordinates file of 5U32 with a resolution of 2.27 Å was secured from RCSB (Research Collaboratory for Structural Bioinformatics) protein data bank [35]. Affinity grids centered on the active site with 126×126×126 grid size with a spacing of 0.42 Å were generated with the aid of AutoGrid 4.2 [36]. The docking procedure was carried out as described in the literature [21]. The docking results were examined through sorting the binding free energy envisaged by the docked confirmations of the semicarbazone **4**. The presaged best confirmation binding energy was −4.02 kcal/mol. The amino acids PHE436, LEU608, ASP607, and LYS610 in the active site of the target

protein binds with the ligand by hydrogen bonding with bond lengths of 1.83 and 2.26 as well as 2.04, 2.27, and 1.92, respectively. The protein-ligand interaction complex is given in Figure 6, suggesting the possible binding mode of the title compound **4** to the target protein 5U32.

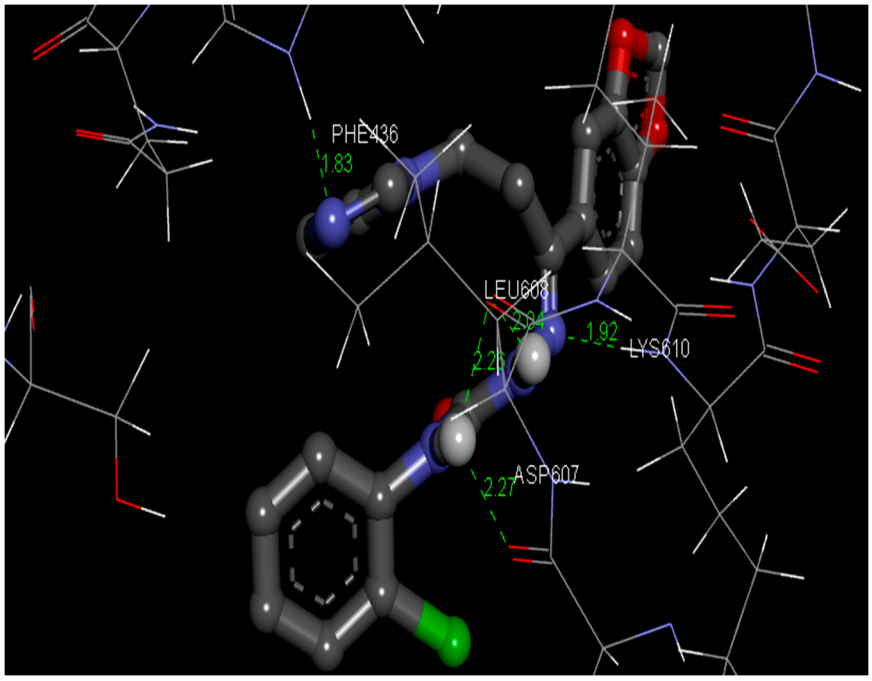


Figure 6. Pose of the semicarbazone **4** with the amino acid residues of the target protein.

3.8. Hirshfeld Surface Analysis

The Hirshfeld surfaces and their associated 2D fingerprint plots for the title compound **4** were computed, taking single crystal X-ray crystal structure as input. The Hirshfeld surface emerged from an attempt to define the space occupied by a molecule in a crystal for the purpose of partitioning the crystal electron density into molecular fragments [37]. It provides a 3D picture of close contacts in a crystal, and these contacts can be summarized in a fingerprint plot [38]. For each point on the Hirshfeld surface, two distances are defined, namely the de: the distance from a point to the nearest nucleus external to the surface and the d_i: the distance to the nearest nucleus internal to the surface. A plot of d_i versus d_e is a 2D fingerprint plot which recognizes the existence of different types of intermolecular interactions. The Hirshfeld surfaces of the title compound are given in Figure 7 and it explains the surfaces that have been mapped over d_{norm}, d_e, and d_i and curvedness (3D plots).

The function d_{norm} (normalized chemical contacts) is a ratio encompassing the distances of any surface point to the nearest d_i and d_e atom and the van der Waals radii of the atoms. The value of d_{norm} may be positive or negative depending on whether the intermolecular contacts being either longer or shorter than the van der Waals separations. The negative value of d_{norm} indicates the sum of d_i and d_e is shorter than the sum of the relevant van der Waals radii, which is considered to be the closest contact and is visualized as red color in the Hirshfeld surfaces. The blue color denotes contacts longer than the sum of van der Waals radii with positive d_{norm} values, whereas contacts close to van der Waalsradiiwith d_{norm} equal to zero are colored white. The intermolecular interactions outwards the H···H/N ··· H/C ··· H/O ··· H bonds as well as the overall fingerprint region of the title molecule are displayed in Figure 8. With these analyses, the division of contributions is possible for different interactions including H ··· H, N ··· H, C ··· H, and O ··· H, which commonly overlap in the full finger print plots. Figure 7 shows the d_{norm} surface of the semicarbazone **4**, highlighting only H ··· H/N ··· H intermolecular contacts. These interactions comprise 35.5% and 5.7% of the total Hirshfeld surface area for this molecule, respectively. O ··· H/N ··· H intermolecular interactions are represented by a two

sharp spike in the 2D fingerprint plot (Figure 8). The relative contributions of the C ··· H and O ··· H contacts are 12.2% and 7.5%, respectively.

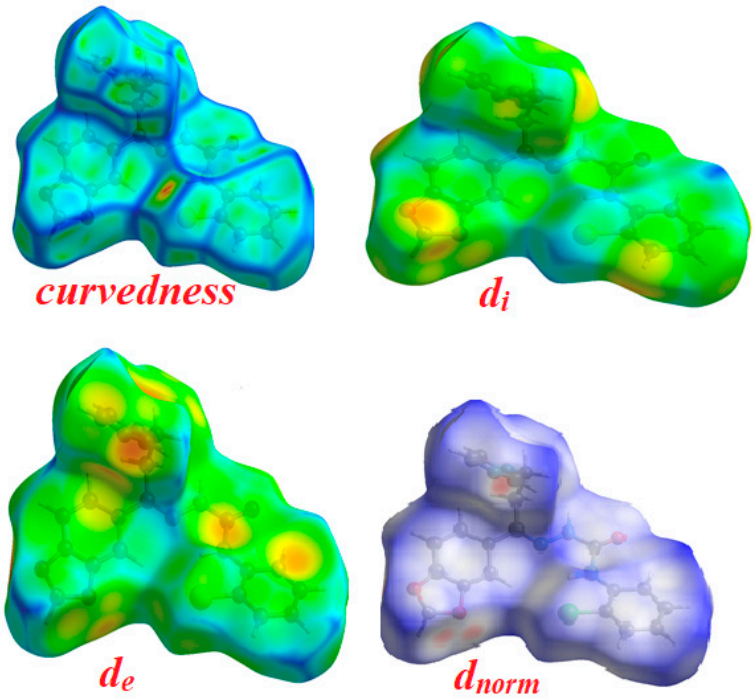


Figure 7. Hirshfeld surfaces for d_{norm}, d_i, and d_e and curvedness for thesemicarbazone **4**.

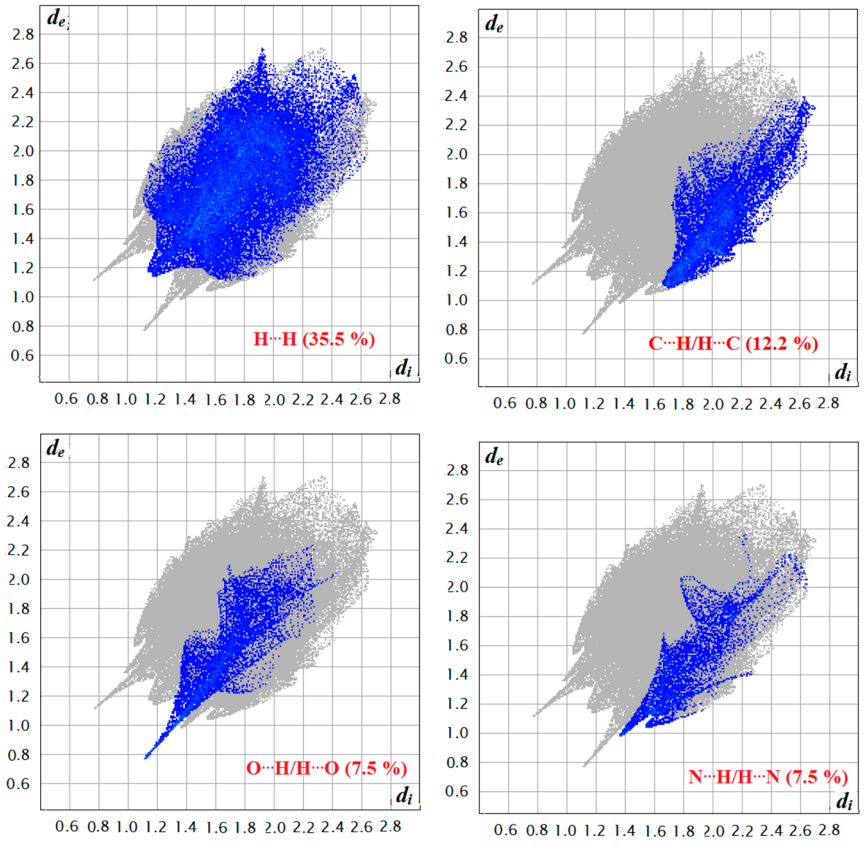


Figure 8. Two dimension finger print plots showing various intermolecular contacts in thesemicarbazones **4**.

3.9. Antifungal Activity of the Semicarbazone **4**

Table 6 illustrates the minimum inhibitory concentrations (MICs) values of the antifungal profile of the target semicarbazone **4,** as well as the reference standard antifungal drugs, fluconazole, and ketoconazole. The best antifungal activity of the semicarbazone **4** was displayed against *C. albicans* with MIC value of 0.156 µmol/mL.

Table 6. The minimum inhibitory concentrations (MICs) values for the antifungal activity of the semicarbazone **4**, fluconazole and ketoconazole towards *Aspergillus niger* and various *Candida* species.

Compound No.	MIC (µmol/mL)			
	C. albicans	*C. tropicalis*	*C.parapsilosis*	*Aspergillus niger*
4	0.156	> 1.24	0.311	0.622
Fluconazole	0.051	0.045	0.047	ND
Ketoconazole	ND	ND	ND	0.02

ND: not determined.

4. Conclusions

(2*E*)-2-[1-(1,3-Benzodioxol-5-yl)-3-(1*H*-imidazol-1-yl)propylidene]-*N*-(2-chlorophenyl) hydrazinecarboxamide (**4**) has been synthesized and identified with different spectroscopic techniques. The assigned chemical structure of the title compound **4** as well as the (*E*)-configuration of its imine functionality were unambiguously assured using single crystal X-ray analysis.

The optimized geometry of the semicarbazone **4** revealed that the predicted values are consistent with the experimental results with few exceptions that are insignificant. The obtained theoretical model of the title compound **4** by DFT calculations describes the possibility of C–H ··· N intramolecular hydrogen bonding and ICT charge transfer interactions that stabilize its structure. These results were further confirmed via NBO and NPA analyses on the title compound **4**. Frontier molecular orbital analysis also confirmed the presence of intramolecular charge transfer within the title molecule **4,** leading to its stability and henceits bioactivity. Hirshfeld surface analysis revealed the occurrence of strong and weak intermolecular interactions in the crystalline state of the semicarbazone **4** like O···H, C···H and N···H bonding. The in vitro antifungal potential of the title compound **4** was examined against different fungal strains and the best activity was manifested against *C. albicans* with MIC value of 0.156 µmol/mL. A molecular docking study suggested the anticipated binding mode of the title compound **4** to its target protein. The results of the current study inspired us to design new antifungal candidates bearing the scaffold of the title compound **4** with the hope of getting more potent antifungal drug-like surrogates with better antifungal profile.

Supplementary Materials: The following are available online at http://www.mdpi.com/2073-4352/9/2/82/s1, Figure S1: Correlation plot for calculated and experimental bond lengths of semicarbazone **4**; Figure S2: ^{1}H NMR spectrum of the semicarbazone **4**; Figure S3: Enlarged part of the ^{1}H NMR spectrum of the semicarbazone **4**; Figure S4:^{13}C NMR spectrum of the semicarbazone **4**.

Author Contributions: R.I.A.-W. and A.R.A.-G. synthesized and characterized the title molecule. H.A.G. conducted X-ray analysis. M.H.A.-A. conducted the antifungal profiling. S.A.V.A. and I.H.J. performed the computational work. M.I.A. conceptualized the work and prepared the manuscript for publication. All authors discussed the contents of the manuscript.

Funding: The authors would like to extend their sincere appreciation to the Deanship of Scientific Research at King Saud University for its funding of this research through the Research Group Project no. RGP-196.

Conflicts of Interest: The authors have declared that there is no conflict of interests.

References

1. Crunkhorn, S. Fungal infection: Protecting from *Candida albicans*. *Nat. Rev. Drug Discov.* **2016**, *15*, 604. [CrossRef] [PubMed]

2. Vandeputte, P.; Ferrari, S.; Coste, A.T. Antifungal resistance and new strategies to control fungal infections. *Int. J. Microbiol.* **2011**, *2012*, 713687. [CrossRef] [PubMed]
3. Wu, J.; Ni, T.; Chai, X.; Wang, T.; Wang, H.; Chen, J.; Jin, Y.; Zhang, D.; Yu, S.; Jiang, Y. Molecular docking, design, synthesis and antifungal activity study of novel triazole derivatives. *Eur. J. Med. Chem.* **2018**, *143*, 1840–1846. [CrossRef] [PubMed]
4. Lino, C.I.; de Souza, I.G.; Borelli, B.M.; Matos, T.T.S.; Teixeira, I.N.S.; Ramos, J.P.; de Souza Fagundes, E.M.; de Oliveira Fernandes, P.; Maltarollo, V.G.; Johann, S. Synthesis, molecular modeling studies and evaluation of antifungal activity of a novel series of thiazole derivatives. *Eur. J. Med. Chem.* **2018**, *151*, 248–260. [CrossRef] [PubMed]
5. Sanglard, D. Emerging threats in antifungal-resistant fungal pathogens. *Front. Med.* **2016**, *3*, 11. [CrossRef] [PubMed]
6. Pappas, P.G.; Kauffman, C.A.; Andes, D.R.; Clancy, C.J.; Marr, K.A.; Ostrosky-Zeichner, L.; Reboli, A.C.; Schuster, M.G.; Vazquez, J.A.; Walsh, T.J. Clinical practice guideline for the management of candidiasis: 2016 update by the Infectious Diseases Society of America. *Clin. Infect. Dis.* **2015**, *62*, e1–e50. [CrossRef]
7. Aoyama, Y.; Yoshida, Y.; Sato, R. Yeast cytochrome P-450 catalyzing lanosterol 14 alpha-demethylation. II. Lanosterol metabolism by purified P-450 (14) DM and by intact microsomes. *J. Biol. Chem.* **1984**, *259*, 1661–1666.
8. Aboul-Enein, M.N.; El-Azzouny, A.A.; Attia, M.I.; Saleh, O.A.; Kansoh, A.L. Synthesis and anti-*Candida* potential of certain novel 1-[(3-substituted-3-phenyl)propyl]-1*H*-imidazoles. *Arch. Pharm.* **2011**, *344*, 794–801. [CrossRef]
9. Roman, G.; Mares, M.; Nastasa, V. A novel antifungal agent with broad spectrum: 1-(4-biphenylyl)-3-(1*H*-imidazol-1-yl)-1-propanone. *Arch. Pharm.* **2013**, *346*, 110–118. [CrossRef]
10. Attia, M.I.; Radwan, A.A.; Zakaria, A.S.; Almutairi, M.S.; Ghoneim, S.W. 1-Aryl-3-(1*H*-imidazol-1-yl)propan-1-ol esters: Synthesis, anti-*Candida* potential and molecular modeling studies. *Chem. Cent. J.* **2013**, *7*, 168. [CrossRef]
11. Venkatachalam, T.K.; Bernhardt, P.V.; Noble, C.J.; Fletcher, N.; Pierens, G.K.; Thurecht, K.J.; Reutens, D.C. Synthesis, characterization and biological activities of semicarbazones and their copper complexes. *J. Inorg. Biochem.* **2016**, *162*, 295–308. [CrossRef] [PubMed]
12. Beraldo, H.; Gambino, D. The wide pharmacological versatility of semicarbazones, thiosemicarbazones and their metal complexes. *Mini Rev. Med. Chem.* **2004**, *4*, 31–39. [PubMed]
13. Jafri, L.; Ansari, F.L.; Jamil, M.; Kalsoom, S.; Qureishi, S.; Mirza, B. Microwave-assisted synthesis and bioevaluation of some semicarbazones. *Chem. Biol. Drug Des.* **2012**, *79*, 950–959. [CrossRef] [PubMed]
14. Laly, S.; Parameswaran, G. Synthesis and characterisation of some thiosemicarbazone complexes of Ag (I), Pt (II) and Pd (II). *Asian J. Chem.* **1993**, *5*, 712–718.
15. Aboul-Enein, M.N.; El-Azzouny, A.A.; Attia, M.I.; Maklad, Y.A.; Amin, K.M.; Abdel-Rehim, M.; El-Behairy, M.F. Design and synthesis of novel stiripentol analogues as potential anticonvulsants. *Eur. J. Med. Chem.* **2012**, *47*, 360–369. [CrossRef] [PubMed]
16. Leite, A.C.L.; da Silva, K.P.; de Souza, I.A.; de Araújo, J.M.; Brondani, D.J. Synthesis, antitumour and antimicrobial activities of new peptidyl derivatives containing the 1,3-benzodioxole system. *Eur. J. Med. Chem.* **2004**, *39*, 1059–1065. [CrossRef] [PubMed]
17. Attia, M.I.; El-Brollosy, N.R.; Kansoh, A.L.; Ghabbour, H.A.; Al-Wabli, R.I.; Fun, H.-K. Synthesis, single crystal X-ray structure, and antimicrobial activity of 6-(1,3-benzodioxol -5-ylmethyl)-5-ethyl-2-{[2-(morpholin-4-yl)ethyl]sulfanyl}pyrimidin-4(3*H*)-one. *J. Chem.* **2014**, *2014*, 457430. [CrossRef]
18. Attia, M.I.; Zakaria, A.S.; Almutairi, M.S.; Ghoneim, S.W. In vitro anti-*Candida* activity of certain new 3-(1*H*-imidazol-1-yl)propan-1-one oxime esters. *Molecules* **2013**, *18*, 12208–12221. [CrossRef] [PubMed]
19. Al-Wabli, R.I.; Al-Ghamdi, A.R.; Ghabbour, H.A.; Al-Agamy, M.H.; Monicka, J.C.; Joe, I.H.; Attia, M.I. Synthesis, X-ray single crystal structure, molecular docking and DFT computations on *N*-[(1*E*)-1-(2*H*-1,3-benzodioxol-5-yl)-3-(1*H*-imidazol-1-yl)propylidene]-hydroxylamine: A new potential antifungal agent precursor. *Molecules* **2017**, *22*, 373. [CrossRef]
20. Al-Wabli, R.I.; Al-Ghamdi, A.R.; Ghabbour, H.A.; Al-Agamy, M.H.; Attia, M.I. Synthesis, single crystal X-ray analysis, and antifungal profiling of certain new oximino ethers bearing imidazole nuclei. *Molecules* **2017**, *22*, 1895. [CrossRef]

21. Al-Wabli, R.I.; Al-Ghamdi, A.R.; Primsa, I.; Ghabbour, H.A.; Al-Agamy, M.H.; Joe, I.H.; Attia, M.I. (2*E*)-2-[1-(1,3-benzodioxol-5-yl)-3-(1*H*-imidazol-1-yl)propylidene]-*N*-(4-methoxyphenyl)hydrazine carboxamide: Synthesis, crystal structure, vibrational analysis, DFT computations, molecular docking and antifungal activity. *J. Mol. Struct.* **2018**, *1166*, 121–130. [CrossRef]
22. Al-Wabli, R.I.; Al-Ghamdi, A.R.; Ghabbour, H.A.; Al-Agamy, M.H.; Attia, M.I. Synthesis and spectroscopic identification of certain imidazole-semicarbazone conjugates bearing benzodioxole moieties: New antifungal agents. *Molecules* **2019**, *24*, 200. [CrossRef] [PubMed]
23. Beukers, M.W.; Wanner, M.J.; Von Frijtag Drabbe Künzel, J.K.; Klaasse, E.C.; Ijzerman, A.P.; Koomen, G.-J. *N*-6-Cyclopentyl-2-(3-phenylaminocarbonyltriazene-1-yl)adenosine (TCPA), a very selective agonist with high affinity for the human adenosine A1 receptor. *J. Med. Chem.* **2003**, *46*, 1492–1503. [CrossRef] [PubMed]
24. Sheldrick, G.M. A short history of SHELX. *Acta Cryst. A* **2008**, *64*, 112–122. [CrossRef] [PubMed]
25. Becke, A.D. Density-functional thermochemistry. III. The role of exact exchange. *J. Chem. Phys.* **1993**, *98*, 5648–5652. [CrossRef]
26. Frisch, M.J.; Trucks, G.W.; Schlegel, H.B.; Scuseria, G.E.; Robb, M.A.; Cheeseman, J.R.; Scalmani, G.; Barone, V.; Mennucci, B.; Petersson, G.A.; et al. *Gaussian-09*; Revision A.02; Gaussian, Inc.: Wallingford, CT, USA, 2009.
27. Jamróz, M.H. Vibrational energy distribution analysis (VEDA): Scopes and limitations. *Spectrochim. Acta Part A Mol. Biomol. Spectrosc.* **2013**, *114*, 220–230. [CrossRef] [PubMed]
28. Wolff, S.; Grimwood, D.; McKinnon, J.; Jayatilaka, D.; Spackman, M. *Crystal Explorer 2.0*; University of Western Australia: Perth, Australia, 2007.
29. Reed, A.E.; Curtiss, L.A.; Weinhold, F. Intermolecular interactions from a natural bond orbital, donor-acceptor viewpoint. *Chem. Rev.* **1988**, *88*, 899–926. [CrossRef]
30. Allen, F.H.; Kennard, O.; Watson, D.G.; Brammer, L.; Orpen, A.G.; Taylor, R. Tables of bond lengths determined by X-ray and neutron diffraction. Part 1. Bond lengths in organic compounds. *J. Chem. Soc. Perkin Trans. 2* **1987**, S1–S19. [CrossRef]
31. Reed, A.E.; Weinstock, R.B.; Weinhold, F. Natural population analysis. *J. Chem. Phys.* **1985**, *83*, 735–746. [CrossRef]
32. Fleming, I. *Frontier Orbitals and Organic Chemical Reactions*; Wiley: Hoboken, NJ, USA, 1977.
33. Morris, G.M.; Huey, R.; Lindstrom, W.; Sanner, M.F.; Belew, R.K.; Goodsell, D.S.; Olson, A.J. AutoDock4 and AutoDockTools4: Automated docking with selective receptor flexibility. *J. Comp. Chem.* **2009**, *30*, 2785–2791. [CrossRef]
34. Bonanno, J.B.; Edo, C.; Eswar, N.; Pieper, U.; Romanowski, M.J.; Ilyin, V.; Gerchman, S.E.; Kycia, H.; Studier, F.W.; Sali, A. Structural genomics of enzymes involved in sterol/isoprenoid biosynthesis. *Proc. Natl. Acad. Sci. USA* **2001**, *98*, 12896–12901. [CrossRef] [PubMed]
35. Bernstein, F.C.; Koetzle, T.F.; Williams, G.J.; Meyer, E.F., Jr.; Brice, M.D.; Rodgers, J.R.; Kennard, O.; Shimanouchi, T.; Tasumi, M. The protein data bank: A computer-based archival file for macromolecular structures. *Arch. Biochem. Biophys.* **1978**, *185*, 584–591. [CrossRef]
36. Morris, G.M.; Goodsell, D.S.; Halliday, R.S.; Huey, R.; Hart, W.E.; Belew, R.K.; Olson, A.J. Automated docking using a Lamarckian genetic algorithm and an empirical binding free energy function. *J. Comp. Chem.* **1998**, *19*, 1639–1662. [CrossRef]
37. Spackman, M.A.; Byrom, P.G. A novel definition of a molecule in a crystal. *Chem. Phys. Lett.* **1997**, *267*, 215–220. [CrossRef]
38. Spackman, M.A.; Jayatilaka, D. Hirshfeld surface analysis. *Cryst. Eng. Comm.* **2009**, *11*, 19–32. [CrossRef]



© 2019 by the authors. Licensee MDPI, Basel, Switzerland. This article is an open access article distributed under the terms and conditions of the Creative Commons Attribution (CC BY) license (http://creativecommons.org/licenses/by/4.0/).